

Original paper

# Astrophyllite–alkali amphibole rhyolite, an evidence of early Permian A-type alkaline volcanism in the western Mongolian Altai

Vladimír ŽÁČEK<sup>1\*</sup>, David BURIÁNEK<sup>1</sup>, Zoltán PÉCSKAY<sup>2</sup>, Radek ŠKODA<sup>1</sup><sup>1</sup> Czech Geological Survey, Klárov 3, 118 21 Prague 1, Czech Republic; vladimir.zacek@geology.cz<sup>2</sup> Institute for Nuclear Research, Hungarian Academy of Sciences (ATOMKI), Bem tér 18/c, Debrecen, Hungary

\*Corresponding author



A dyke of alkali rhyolite intrudes the Tsetseg and Zuun Nuruu volcanosedimentary sequence of Ordovician–Silurian age (Hovd Zone, Central Asian Orogenic Belt) at the Botgon bag, Mankhan Soum, Hovd District in Western Mongolia. The rock consists of quartz and K-feldspar phenocrysts set in fine-grained groundmass composed of quartz, K-feldspar, albite, blue alkali amphibole (riebeckite–arfvedsonite containing up to 1.94 wt. % ZrO<sub>2</sub>), tiny brown radial astrophyllite, annite and accessory zircon, ilmenite, fluorite, monazite, hematite, chevkinite and bastnäsite. Astrophyllite has unusual, highly ferroan composition and occurs as two sharply bound zones of astrophyllite I and II with the average empirical formulae: (K<sub>1.71</sub>Na<sub>0.01</sub>Rb<sub>0.08</sub>Cs<sub>0.01</sub>)(Na<sub>0.93</sub>Ca<sub>0.07</sub>)(Fe<sup>2+</sup><sub>6.52</sub>Mn<sub>0.31</sub>Zn<sub>0.06</sub>)(Ti<sub>0.84</sub>Zr<sub>0.50</sub>Nb<sub>0.55</sub>)Si<sub>7.68</sub>Al<sub>0.32</sub>O<sub>26</sub>(OH)<sub>3.78</sub>F<sub>0.66</sub> (astrophyllite I, Zr–Nb-rich); (K<sub>1.52</sub>Rb<sub>0.07</sub>)(Na<sub>0.81</sub>Ca<sub>0.19</sub>)(Fe<sup>2+</sup><sub>6.31</sub>Mn<sub>0.28</sub>Zn<sub>0.06</sub>)(Ti<sub>1.28</sub>Nb<sub>0.30</sub>Zr<sub>0.28</sub>)Si<sub>7.68</sub>Al<sub>0.32</sub>O<sub>26</sub>(OH)<sub>2.85</sub>F<sub>0.67</sub> (astrophyllite II). Geochemically, the rhyolite corresponds to strongly fractionated silicic alkaline A-type (ferroan) magmatic rock with 75.5–75.9 wt. % SiO<sub>2</sub>, 4.4 wt. % K<sub>2</sub>O, 3.9–4.3 wt. % Na<sub>2</sub>O and 1.98–2.23 wt. % Fe<sub>2</sub>O<sub>3</sub><sup>t</sup>, poor in CaO (0.26–0.37 wt. %), MgO (0.01–0.11 wt. %), and P<sub>2</sub>O<sub>5</sub> (0.01 wt. %). The rock is enriched in Zr, Nb, Ta, Ga, Sn, Y, Rb, Cs, U and Th, depleted in V, Sr, Ba, Sc, and exhibits a pronounced negative Eu anomaly (Eu/Eu\* = 0.03–0.05). The conventional whole-rock K–Ar geochronology yielded an age of 299.9 ± 9.1 Ma (1σ), which indicates latest Carboniferous or early Permian extension associated with the A-type alkaline volcanic activity.

**Keywords:** rhyolite, A-type, astrophyllite, K–Ar geochronology, CAOB

**Received:** 29 October, 2015; **accepted:** 12 January, 2016; **handling editor:** K. Schulmann

## 1. Introduction

The Central Asian Orogenic Belt (CAOB, Şengör et al. 1993; Jahn et al. 2000) is located between Uralian Orogen in the west, Siberian Craton in the north, Tarim Craton in the southwest and Sino-Korean Craton in the south. The CAOB represents the largest accretionary system on the Earth (~8000 × 6000 km) formed as a result of the subduction and closure of the Paleo-Asian Ocean (Zonenshain et al. 1990; Şengör et al. 1993; Jahn et al. 2000; Buslov et al. 2001). The CAOB is a complex “collage” of continental blocks, accretionary wedges, magmatic arcs, back-arcs and fragments of oceanic crust amalgamated during the Paleozoic to Mesozoic eras (Şengör et al. 1993).

The Late Paleozoic rift-related intrusive and extrusive acid igneous rocks are relatively common in northern China and south-western Mongolia (Wang ZG et al. 1993; Litvinovsky et al. 2002; Wu et al. 2002; Chen and Jahn 2004; Jahn 2004; Chen and Arakawa 2005; Wang Q et al. 2007; Buriánek et al. 2012; Liu et al. 2013; Mao et al. 2014). These generally undeformed, anorogenic-type intrusions provide evidence of the final amalgamation of terranes in this part of the CAOB (Jahn 2004; Liu et al. 2013; Mao et al. 2014).

This paper is intended to provide new geochemical and geochronological data on the astrophyllite- and alkali amphibole-bearing rhyolite dyke cutting the Lower Paleozoic volcanosedimentary and plutonic sequence in the Hovd Zone in Western Mongolia.

## 2. Geological setting

The study area is situated near the boundary between two terranes: (1) the Lake Zone to the east and (2) the Hovd Zone to the west (Badarch et al. 2002, Fig. 1). These domains are separated from each other by an important crustal-scale boundary, which was interpreted as a wide strike-slip fault zone (Tomurtogoo 1997).

The Lake Zone is a composite terrane, which contains Neoproterozoic to Cambrian volcanosedimentary complexes and ophiolites intruded by Late Cambrian–Middle Ordovician syn- to post-tectonic gabbro, diorite, granodiorite and granite (Kovalenko et al. 1996; Kröner et al. 2010; Soejono et al. this volume). The Hovd Zone is interpreted as a part of the accretionary wedge (e.g., Xiao et al. 2004, details in Soejono et al. this volume) and is composed of several lithostratigraphic units of documented or supposed Ordovician to Silurian ages

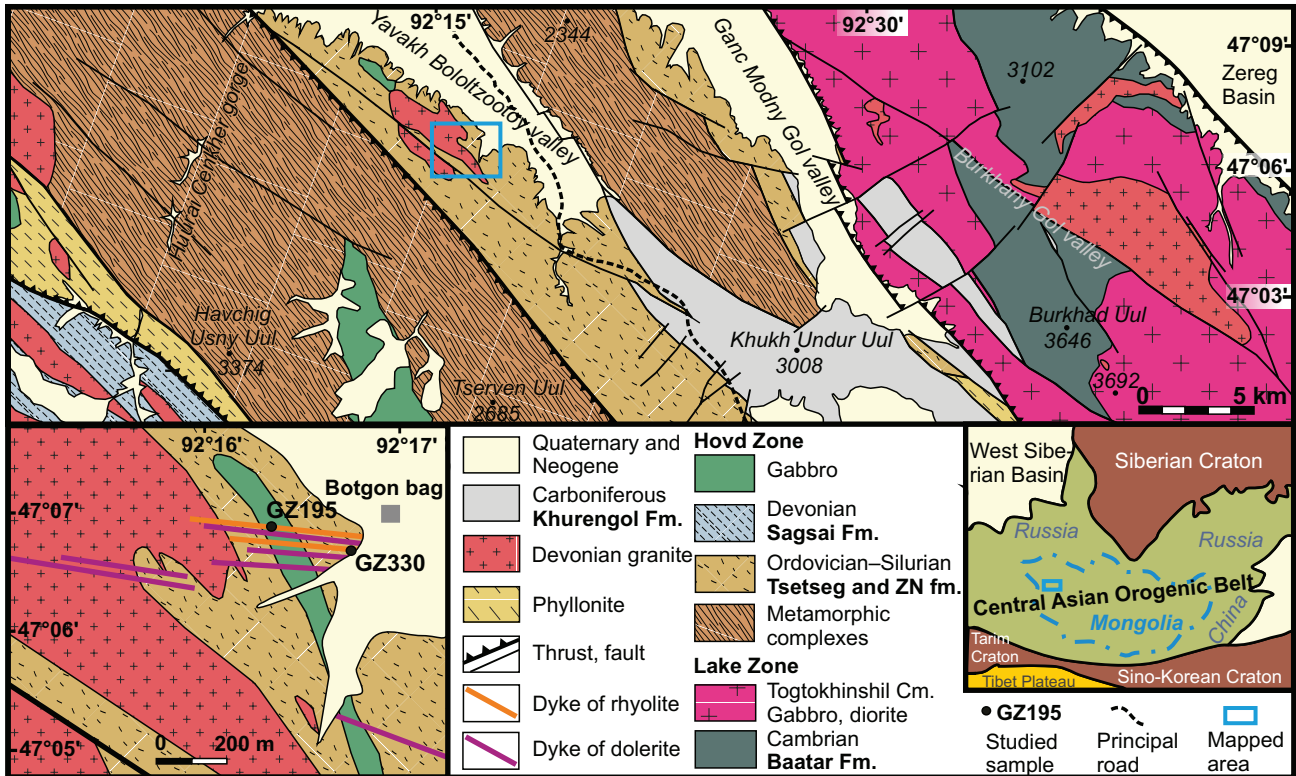


Fig. 1 Geological structure of the wider area around the alkali rhyolite occurrence depicted from recent (2015) manuscript geological maps 1:50 000 of the Czech Geological Survey. Abbreviations used: ZN – Zuun Nuruu, Cm. – Complex, Fm. – Formation.

(Baatarhuyag and Gansukh 1999). Also, the existing geochronological studies mostly from the Chinese Altai suggest these rocks to have been deposited during the Ordovician to the Silurian (Sun et al. 2008; Long et al. 2009). Lithologically, the Hovd Zone is composed mainly of pelitic schists intercalated with basic volcanic rocks and fossiliferous carbonate lenses. Greenschist- to amphibolite-facies metamorphism occurred during an Early Devonian event as shown by a study of zircon in the Habahe Group in the adjacent Tsel Terrane (Jiang et al. 2010, 2012). This sequence is crosscut by various granitic, dioritic to gabbroic intrusions, mostly syn-metamorphic. Numerous U–Pb zircon ages from similar calc-alkaline granitic rocks of the Habahe Group suggest Devonian to early Carboniferous age of the major magmatic pulse (Jiang et al. 2010). The youngest formation consists of Lower Carboniferous siliciclastic sediments deposited in a syn-orogenic basin.

### 3. Methods

#### 3.1. Field work

Field work was carried out and relevant material and samples collected in June–July 2014, and 2015. During the field mapping, all important structural data were

documented, and the KT-10 kappameter was used to measure the magnetic susceptibility.

#### 3.2. Whole-rock geochemistry

The whole-rock analyses were performed in Activation Laboratories (Actlabs; Toronto, Canada) using the procedure 4Lithoresearch (<http://www.actlabs.com>). Major-element concentrations were obtained by inductively-coupled plasma optical emission spectrometry (ICP-OES), trace-element concentrations were established by inductively-coupled plasma mass spectrometry (ICP-MS). Subsequently, the sample GZ195 was analyzed in Laboratories of the Czech Geological Survey in Prague (using the material pulverized in the Actlabs) to determine FeO, Fe<sub>2</sub>O<sub>3</sub>, Li<sub>2</sub>O, and F (Tab. 1). Geochemical data were recalculated and plotted by the *GCDkit* software package (Janoušek et al. 2006).

#### 3.3. Electron microprobe analyses (EMPA)

Electron-microprobe analyses of minerals (sample GZ195) were carried out using a Cameca SX-100 electron microprobe in the Joint laboratory of the Masaryk University and of the Czech Geological Survey in Brno. The astrophyllite and amphibole were

**Tab. 1** Whole-rock geochemical analyses of the alkali rhyolite (wt. %, ppm)

sample	GZ195	GZ330	sample	GZ195	GZ330
SiO <sub>2</sub>	75.52	75.93	Fe <sub>2</sub> O <sub>3</sub>	1.42	–
Al <sub>2</sub> O <sub>3</sub>	11.63	11.77	FeO	1.6	–
Fe <sub>2</sub> O <sub>3</sub> <sup>t</sup>	1.98	2.23	Li <sub>2</sub> O	0.017	–
MnO	0.029	0.034	F	0.161	–
MgO	0.11	0.01	Cs	6.2	4.7
CaO	0.37	0.26	Rb	207	207
Na <sub>2</sub> O	3.94	4.35	Sr	14	3
K <sub>2</sub> O	4.49	4.43	Ba	40	11
TiO <sub>2</sub>	0.125	0.088	Be	9	9
P <sub>2</sub> O <sub>5</sub>	0.01	< 0.01	Th	23.8	18.9
LOI	0.62	0.04	U	4.50	4.21
Total	98.82	99.16	Zr	422	375
A/CNK	0.97	0.95	Hf	14.0	10.9
A/NK	1.03	0.98	Nb	82.6	53.3
Na <sub>2</sub> O/K <sub>2</sub> O	0.88	0.98	Ta	7.61	6.12
Y	92.6	109.0	Pb	43	32
La	37.0	39.6	Bi	0.2	0.2
Ce	90.1	94.0	Ag	5.1	0.7
Pr	10.9	11.3	Cu	20	< 10
Nd	41.2	42.8	Zn	190	170
Sm	11.8	12.4	Mo	< 2	< 2
Eu	0.20	0.15	As	28	< 5
Gd	12.8	14.4	Sn	18	11
Tb	2.62	2.85	V	10	< 5
Dy	16.6	18.7	Cr	90	< 20
Ho	3.29	3.73	Co	< 1	< 1
Er	9.98	11.2	Ni	< 20	< 20
Tm	1.64	1.63	Sc	< 1	< 1
Yb	10.4	10.6	In	< 0.1	0.1
Lu	1.54	1.53	Sb	0.6	< 0.2
Eu/Eu*	0.05	0.03	Ga	36	32
La <sub>N</sub> /Yb <sub>N</sub>	2.4	2.5	Ge	2.9	2.4
La <sub>N</sub> /Sm <sub>N</sub>	2.0	2.3	W	< 0.5	1.2
ΣREE	250.01	265.89	Tl	1.0	0.9

measured at conditions: accelerating voltage 15 kV, beam current 10 nA and beam diameter 8 μm. The following lines, monochromators and standards were used: F (K<sub>α</sub>, PC1, topaz); Si, K, Al (K<sub>α</sub>, TAP, sanidine); Mg (K<sub>α</sub>, TAP, pyrope); Na (K<sub>α</sub>, TAP, albite); Rb (L<sub>α</sub>, TAP, synthetic Rb-leucite); Zr (L<sub>α</sub>, TAP, zircon); Ti (K<sub>α</sub>, PET, anatase); Ca (K<sub>α</sub>, PET, wollastonite); Cl (K<sub>α</sub>, PET, vanadinite); Nb (L<sub>α</sub>, PET, columbite-Fe); Cs (L<sub>α</sub>, PET, pollucite); Fe (K<sub>α</sub>, LIF, almandine); Mn (K<sub>α</sub>, LIF, spessartine); V (K<sub>α</sub>, LIF, ScVO<sub>4</sub>); Zn (K<sub>α</sub>, LIF, gahnite). Chromium, P, Y, La, Dy and Yb were sought but not detected. Peak-counting times were 10 and 20 s for major elements and 30 and 40 s for minor to trace elements. Raw intensities were processed by X-PHI matrix correction (Merlet 1994). Natural minerals and stable synthetic compounds were used for analyses of other minerals; beam diameter was 3 μm for zircon and 5 μm for other minerals.

### 3.4. K-Ar geochronology

The age determination was made by conventional K–Ar method in ATOMKI, Debrecen, Hungary. Sample of rhyolite for the dating (GZ195) was prepared in the laboratories of the Czech Geological Survey in Prague. After the crushing, the whole-rock fraction of 0.125–0.30 mm (50–100 g) was washed several times in distilled water, and subsequently dried at 40 °C.

#### 3.4.1. Potassium determination

Approximately 0.05 g of finely pulverized sample was digested in acids (HF, HNO<sub>3</sub> and H<sub>2</sub>SO<sub>4</sub>) in Teflon beakers and finally dissolved in 0.2 M HCl. Potassium was determined by flame photometry with a Na buffer and Li internal standard using Industrial M420 type flame photometer. Multiple runs of inter-laboratory standards (Asia1/95, LP-6, HD-B1, GL-0) indicated the accuracy and reproducibility of this method to be within 2 %.

#### 3.4.2. Argon measurements

Approximately 0.5 g of the sample was wrapped in an aluminium foil and copper sieve preheated for about 24 h at 150–180 °C in a vacuum. Argon was extracted under ultra-high vacuum conditions by RF (high frequency) induction heating and fusion of rock samples in Mo crucibles. The gas was purified by Ti sponge and SAES St 707 type getters to remove chemically active gas contaminants in addition to liquid nitrogen in cold trap to remove condensable gases. The extraction line is linked directly to a mass spectrometer (90° magnetic sector, 155 mm radius, equipped with a Faraday cap), used in static mode.

Argon isotope ratios were measured by the <sup>38</sup>Ar isotope dilution mass spectrometric method, previously calibrated with atmospheric argon and international rock standards.

Experimental details and results of calibration have been described by Balogh (1985). The age of the samples is calculated using the decay constants suggested by Steiger and Jäger (1977). Analytical error is given at 68 % confidence level (1σ) using the equation of Cox and Dalrymple (1967).

## 4. Results

### 4.1. Field observations

The rhyolite was sampled at two sites, both situated on the southern slope of a valley at the Botgon bag in Mankhan Soum, Hovd District in Western Mongo-

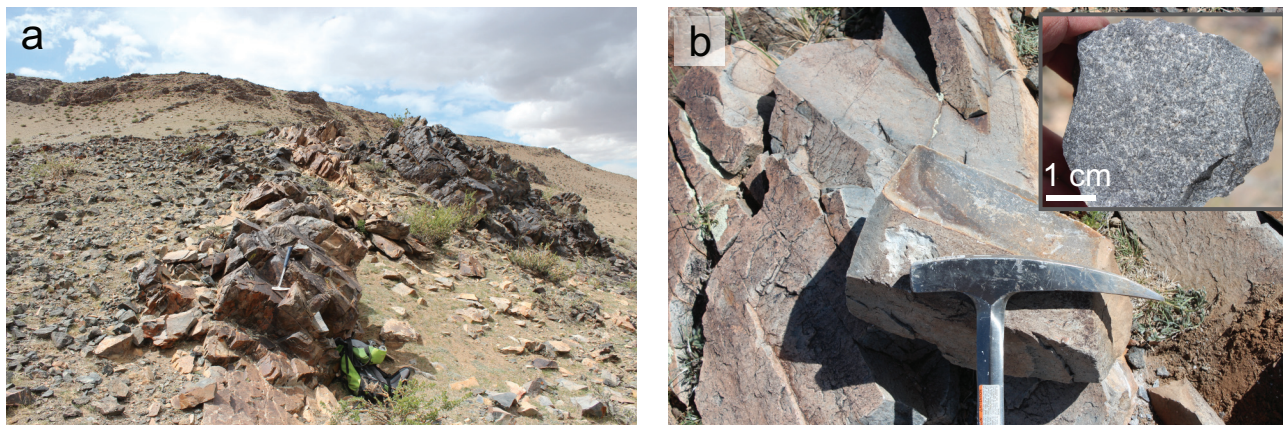


**Fig. 2** Exposure of a rhyolite dyke at Botgon bag. **a** – Rhyolite dyke forms conspicuous, light-coloured rocky wall, and cuts the gabbro and quartzite schist of the Tsetseg and Zuun Nuruu formations of the Ordovician to Silurian ages (see Fig. 1). **b** – Sampling site and hand-specimen of sample GZ195.

lia. Samples GZ195 and GZ330 were taken from two individual WNW–ESE striking ~2–5 m thick dykes, which cut with evident discordancy the gabbro, biotite schists, quartzite schists, quartzites, and porphyritic biotite granite (Fig. 2a). The schists, quartzite and gabbro belong to the Tsetseg and Zuun Nuruu formations of Silurian to Ordovician ages (Baatarhuyag and Gansukh 1999); the granite is likely of Devonian age. The studied rhyolite dykes are accompanied by a dyke swarm 300 m wide consisting of doleritic dykes up to ~15 m thick, all of which show the same strike (Fig. 1). However, while the dolerite dykes are common and distributed over much of the area mapped, alkali rhyolite was observed only at the locality studied.

#### 4.2. Petrography

The rhyolite is fresh, massive, greyish in colour, and contains quartz and feldspar phenocrysts visible to the eye, 1–3 mm long (Fig. 2). The rock displays low magnetic susceptibility of  $0.03\text{--}0.20 \times 10^{-3}$  SI. In thin sections, a weak magmatic foliation is apparent (Fig. 3a). The mineral assemblage consists of quartz + K-feldspar + albite with minor alkali amphibole (2–3 vol. %), astrophyllite (1–2 %), annite (~1 %) and several accessory minerals.

Under the microscope, the rock consists of perthitic microcline phenocrysts 1–3 mm long (~3 vol. %), and minute quartz phenocrysts nearly 1 mm long (~5 vol. %). The groundmass (recrystallized glass, ~80 vol. %) is composed of a granophyric intergrowth of alkali feldspar and quartz, 0.2–0.3 mm in size, along with minute grains of quartz (Fig 3b). Strongly pleochroic blue alkali amphibole forms 0.01–0.2 mm long prismatic to stubby aggregates (Fig. 3c). Bright brown astrophyllite clusters into radial aggregates composed of prismatic to acicular crystals up to 0.3 mm long (Fig. 3d). Greenish-black flakes of annite are prismatic to irregular, up to 0.5 mm

long. Accessory minerals include abundant zircon, minor monazite and REE-rich fluorite as well as rare Ca, Fe, Ti, Ce silicate, presumably chevkinite, and Ca-poor, F-rich, REE-bearing carbonate, possibly bastnäsite. Zircon forms euhedral stubby crystals or their angular fragments up to ~100  $\mu\text{m}$  long. Monazite occurs as subhedral grains up to ~60  $\mu\text{m}$ , and ?chevkinite was found as single 10  $\mu\text{m}$  long inclusion in zircon. Inclusions of ?bastnäsite, ~1–5  $\mu\text{m}$  across, and up to 25  $\mu\text{m}$  long inclusions of REE-rich fluorite in alkali amphibole were identified by EDX. Hematite was encountered in a unique miarolitic structure filled with quartz, annite and minor hematite, the latter forming ~40  $\mu\text{m}$  hexagonal tabular crystals.

#### 4.3. Mineral chemistry

**Sodic amphibole** shows weak irregular zoning apparent in BSE images (Fig. 3e); the zoning has a character of metasomatic replacement. The dominant darker and most probably older amphibole has low Zr content (0.00–0.02 apfu), whereas the lighter zones correspond to younger, Zr-enriched compositions (0.05–0.22 apfu Zr). However, some intermediate compositions can be observed (Fig. 3e, Tab. 2). The sodic amphibole is Fe-dominant with low Mn (0.06–0.08 apfu), Mg (0.00–0.02 apfu), and Ti (0.02–0.12 apfu), see Tab. 2. The standard normalization procedures of EMPA data yielded non-stoichiometric formulae with Si = 8.02–8.22 apfu, perhaps reflecting the possible presence of Li in the amphibole. Direct measurement of Li by LA ICP-MS was not possible due to small size of the amphiboles. The tentative formula calculated, assuming Si = 8 apfu, yielded a minimum  $\text{Li}_2\text{O}$  content 0.03–0.6 wt. %, which corresponds to 0.02–0.42 Li apfu (Tab. 2). The nomenclature of this alkali amphibole is therefore complicated due to variable  $(\text{Na} + \text{K})_{\text{A}}$  occupancies (0.27–0.66 apfu), and possible presence of Li. Principally, the amphibole composition varies between

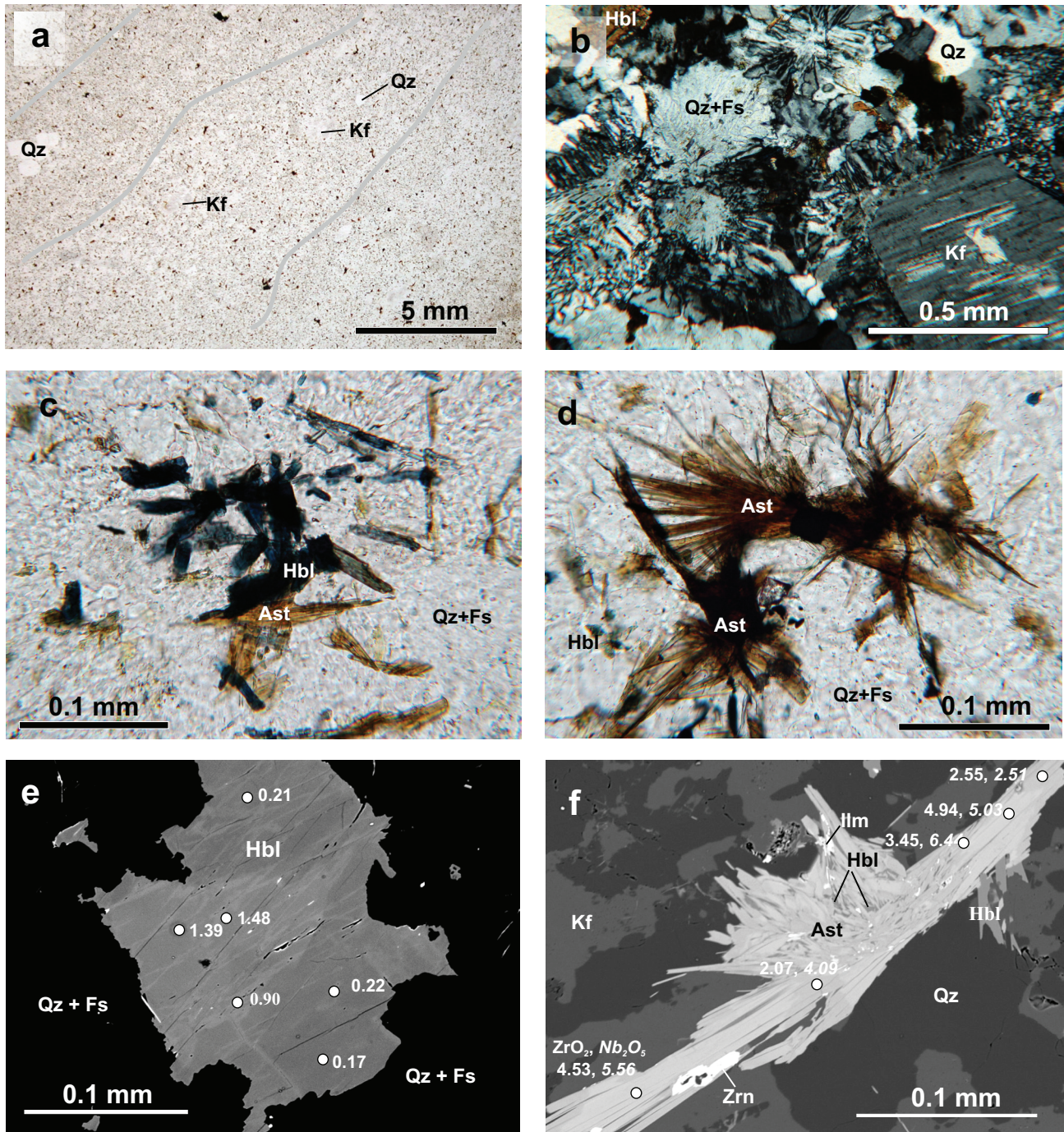


**Fig. 3** Microscopic (a–d) and BSE images (e–f) of sample GZ195. **a** – Weak magmatic foliation (highlighted by grey lines) indicated by alternation of finer and coarser zones. The tiny semi-opaque inclusions are alkali amphibole, astrophyllite and annite (plane polarized light). **b** – Micrographic (granophytic) structure due to rapid cooling of the rhyolite melt (crossed nicols). **c** – A group of blue prismatic to stubby crystals of alkali amphibole associated with minor brownish prismatic to acicular crystals of astrophyllite (plane polarized light). **d** – Radial aggregates of acicular astrophyllite crystals associated with minor alkali amphibole. The associated minerals form intimate intergrowths of quartz and alkali feldspars (plane polarized light). **e** – Large corroded phenocryst of alkali amphibole with EMPA spots labelled by  $ZrO_2$  concentrations (wt. %). The crystal of alkali amphibole displays zoning indicated by alternation of lighter streaks and patches, and relict darker domains. Lighter zones are strongly enriched in Zr (up to 1.48 wt. %  $ZrO_2$ ), whereas dark domains contain only ~0.20 wt. %  $ZrO_2$ . Tiny white inclusions consist of REE-carbonate, possibly bastnäsite. **f** – Radial aggregate of astrophyllite with EMPA spots showing concentrations of  $ZrO_2$  and  $Nb_2O_5$  (in *italic*) (both in wt. %). Associated minerals include alkali amphibole, in places replaced by astrophyllite, quartz, potassium feldspar, and accessory ilmenite. The astrophyllite shows sector zoning, the darker zones represent mostly marginal parts of the crystals and have lower concentrations of both Nb and Zr. Abbreviations used: Hbl – alkali amphibole, Ast – astrophyllite, Qz – quartz, Kf – potassium feldspar, Fs – alkali feldspars, Ilm – ilmenite, Zrn – zircon.

**Tab. 2** Chemical composition of alkali amphibole (wt. %)

zone	dark	dark	dark	light	light	light
SiO <sub>2</sub>	51.72	50.93	51.00	50.36	50.42	51.17
TiO <sub>2</sub>	0.13	0.78	0.53	0.92	0.77	0.43
ZrO <sub>2</sub>	0.00	0.17	0.25	0.90	1.39	1.94
Al <sub>2</sub> O <sub>3</sub>	1.42	0.83	0.80	1.06	0.82	0.81
Fe <sub>2</sub> O <sub>3</sub> calc	12.83	10.60	12.08	9.75	9.11	11.42
FeO calc	21.43	23.23	21.87	24.84	23.82	21.15
MnO	0.51	0.51	0.44	0.43	0.60	0.51
ZnO	0.30	0.61	0.53	0.59	0.60	0.42
MgO	0.07	0.01	0.02	0.04	0.02	0.06
CaO	0.14	0.14	0.16	0.17	0.15	0.15
Li <sub>2</sub> O calc	0.55	0.47	0.56	0.03	0.38	0.66
Na <sub>2</sub> O	7.49	7.86	7.48	6.50	7.51	7.11
K <sub>2</sub> O	1.36	1.21	1.42	1.15	1.20	1.61
F	1.57	2.02	1.63	0.64	1.85	1.85
H <sub>2</sub> O calc	1.19	0.95	1.15	1.61	1.03	1.04
-O=F	-0.66	-0.85	-0.69	-0.27	-0.78	-0.78
total	100.71	100.32	99.92	98.99	99.67	100.33
Si	8.000	8.000	8.000	8.000	8.000	8.000
Ti	0.016	0.092	0.063	0.110	0.092	0.050
Zr	0.000	0.013	0.019	0.070	0.107	0.148
Al	0.258	0.153	0.147	0.199	0.152	0.149
Fe <sup>3+</sup>	1.494	1.252	1.428	1.165	1.088	1.342
Zn	0.035	0.071	0.061	0.069	0.070	0.048
Mn <sup>2+</sup>	0.066	0.068	0.058	0.058	0.081	0.067
Fe <sup>2+</sup>	2.772	3.051	2.868	3.300	3.160	2.767
Mg	0.016	0.002	0.006	0.009	0.004	0.014
Li	0.344	0.297	0.350	0.019	0.244	0.415
C subtotal	5.001	4.999	5.000	4.999	4.998	5.000
Ca	0.023	0.023	0.027	0.029	0.025	0.025
Na	1.977	1.977	1.973	1.971	1.975	1.975
B subtotal	2.000	2.000	2.000	2.000	2.000	2.000
Na	0.269	0.415	0.300	0.032	0.335	0.181
K	0.269	0.243	0.284	0.233	0.244	0.322
A subtotal	0.538	0.658	0.584	0.265	0.579	0.503
O	22.000	22.000	22.000	22.000	22.000	22.000
OH	1.232	0.995	1.190	1.681	1.073	1.084
F	0.768	1.005	0.810	0.319	0.927	0.916

normalization scheme based on 22 O, 2 (OH + F),  $T + C = 13$

Li calculated for 8 Si apfu showing the minimum content of Li in the formula

riebeckite (which has theoretically  $(Na + K)_A = 0$  apfu) and arfvedsonite (with theoretical  $(Na + K)_A = 1.0$  apfu). Nevertheless, if Li exceeds 0.5 apfu, then the amphibole should be classed as ferroleakeite.

**Astrophyllite** shows a sharp sector- to patchy growth zoning in the BSE image. The lighter sectors (astrophyllite I) are significantly richer both in Zr and Nb than the darker ones that are mostly marginal (astrophyllite II, Fig. 3f). A proportion of 31 (O + OH + F) assuming 5 atoms of (OH + F) was used for calculation of astrophyllite formula. A general empirical formula proposed by Piilonen et al. (2000):  $A_2BC_7D_2T_8O_{26}(OH)_4X$  was applied, where  $A = K, Na, Rb, Cs$ ;  $B = Na, Ca$ ;  $C = Fe^{2+}, Fe^{3+}, Mn, Mg, Zn$ ;  $D = Ti, Nb, Zr$ ;  $T = Si$ , and  $X = F, OH$ . Piilonen et al.

(2000) also stated that the  $Fe^{3+}/Fe^t$  values are low, and following the Mössbauer spectroscopy range from 0.01–0.21, corresponding to 0.05–0.56 apfu  $Fe^{3+}$ . Therefore, all iron is considered here to be  $Fe^{2+}$ .

Astrophyllite (both I and II) exhibits an atypical chemical composition. It is classified as astrophyllite on the basis of prevailing cation at C-site (Fe), but with high  $Fe_{tot}/(Fe_{tot} + Mn)$  ratio of 0.95–0.96 (Fig. 4a). The contents of Nb and Zr are also elevated, so that in the diagram depicting the astrophyllite group based on D-site occupancy, the compositions of astrophyllite I are plotted in the proximity of “Fe-zircophyllite” and niobophyllite fields (Fig. 4b) (Kapustin 1972; Piilonen et al. 2000, 2003; Sokolova 2012, see also Tab. 3).

The resulting average empirical formula of astrophyllite I (Zr–Nb-rich) corresponds to:  $(K_{1.71}Na_{0.01}Rb_{0.08}Cs_{0.01})(Na_{0.93}Ca_{0.07})(Fe^{2+}_{6.52}Mn_{0.31}Zn_{0.06})(Ti_{0.84}Zr_{0.50}Nb_{0.55})Si_{7.68}Al_{0.32}O_{26}(OH)_{3.78}F_{0.66}$ . In comparison, the average formula of astrophyllite II is:

$(K_{1.52}Rb_{0.07})(Na_{0.81}Ca_{0.19})(Fe^{2+}_{6.31}Mn_{0.28}Zn_{0.06})(Ti_{1.28}Nb_{0.30}Zr_{0.28})Si_{7.68}Al_{0.32}O_{26}(OH)_{2.85}F_{0.67}$ .

**Annite** has a composition close to the end-member formula, slightly enriched in Rb and Zn:  $(K_{1.01}Na_{0.02}Rb_{0.02})(Fe^{2+}_{2.11}Mg_{0.03}Mn_{0.03}Zn_{0.04})Al_{1.06}Si_{3.41}OH_{1.16}F_{0.84}$ . The mica is purely ferroan,  $Mg/(Mg + Fe^t) = 0.016$ . The phenocrysts of **potassium feldspar** ( $Or_{98}Ab_2$ ) contain ~0.1 wt. % FeO, whereas the ground-mass K-feldspar ( $Or_{98}Ab_2$ ) is slightly richer in this oxide (0.31–0.39 wt. % FeO). **Plagioclase** is represented by albite ( $Ab_{95}Or_5$ ) slightly enriched in FeO

(0.39 %), and  $Rb_2O$  (0.11 wt. %). The concentrations of oxides of Ba, Sr, Cs, and P are below 0.02 wt. % in all feldspars.

**Zircon** contains elevated Th (0.012–0.035 apfu), U (0.003–0.007 apfu), Y (0.011–0.034 apfu), moderate Hf (0.013–0.014 apfu) and  $\Sigma REE$  (0.018–0.032 apfu).

#### 4.4. Whole-rock geochemistry

The rhyolite ( $SiO_2 = 75.52$  and  $75.93$  wt. %) is ferroan ( $FeO^t/(FeO^t + MgO) = 0.94$ – $1.00$  by weight; Fig. 5a), alkali-calcic ( $Na_2O + K_2O - CaO = 8.06$ – $8.52$  wt. %; Fig. 5b), and metaluminous ( $A/CNK = 0.81$ – $0.97$ ), with

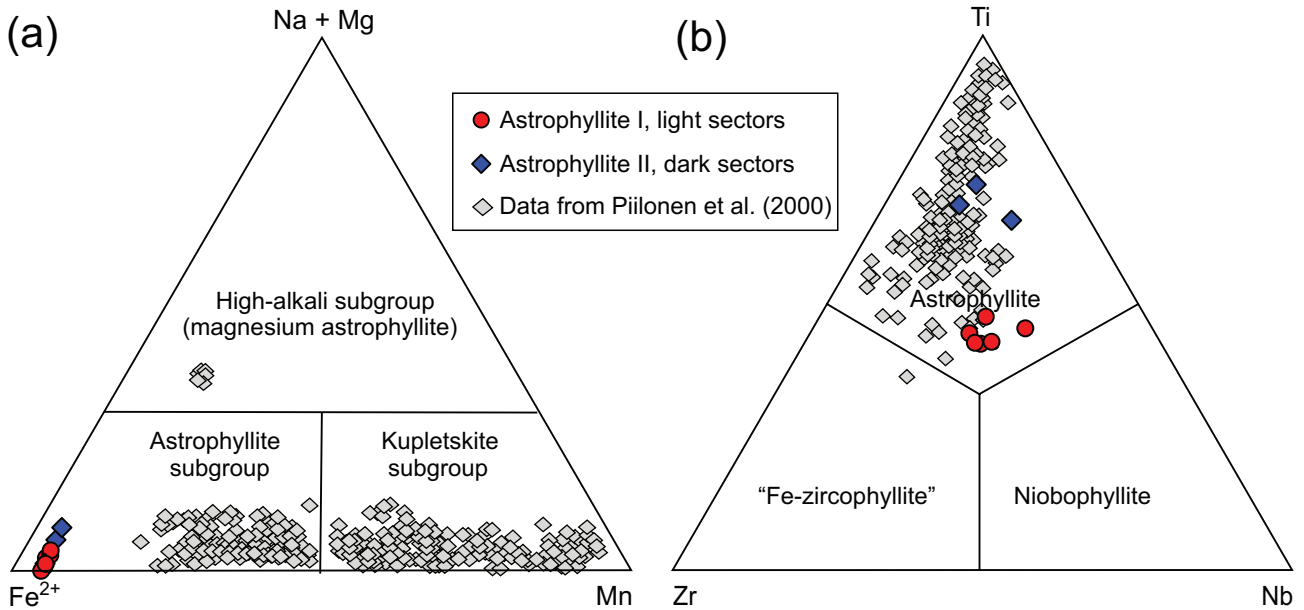


**Fig. 4** Chemical composition of astrophyllite from the Botgon bag, Mongolia, compared with 695 EMP compositions reported by Piilonen et al. (2000). **a** – Ternary C-site Fe<sup>2+</sup> – (Na + Mg) – Mn classification diagram. **b** – Ternary D-site Zr – Ti – Nb classification diagram for minerals of the astrophyllite group (both diagrams after Piilonen et al. 2000). Note the anomalous, extremely ferroan composition of astrophyllite in Fig. 4a, and the Zr + Nb enrichment in astrophyllite I (Fig. 4b).

a low MgO content (0.01–0.11 wt. %). The rhyolite is enriched in most of the LILE (e. g. Rb, K), HFSE (e. g. Th, Zr, Nb, Ta) and depleted in Ba, P, Sr and Ti when observed on the primitive mantle-normalized multi-element pattern (McDonough and Sun 1995; Fig. 6a). The chondrite-normalized REE pattern (Fig. 6b) shows higher proportion of LREE over HREE ( $La_N/Yb_N = 2.40\text{--}2.52$ ), pronounced negative Eu anomaly ( $Eu/Eu^* = 0.03\text{--}0.05$ ) and a M-type tetrad effect ( $TE_{1-3} = 1.13\text{--}1.14$ ; the degree of the lanthanide tetrad effect *sensu* Irber 1999).

The relatively high content of Zr (375–422 ppm), Nb (53–82 ppm), Ce (90–94 ppm; Fig. 7a), and Y (93–109 ppm; Fig. 7b), as well as the elevated  $10000 \times Ga/Al$  ratios of 5.1 and 5.8 indicate an A-type affinity for the rhyolite (Whalen 1987; Bonin 2008).

In the diagram  $(Na_2O + K_2O) - Fe_2O_3 \times 5 - (CaO + MgO) \times 5$  (Fig. 7c) for classification of the A-type (ferroan) granites (Grebennikov 2014), the rhyolite falls along the boundary between the field of A<sub>1</sub>-type granite (silicic rocks of within-plate geodynamic settings: ocean islands and continental rifts)

and A<sub>2</sub>-type granite (silicic rocks of post-collisional and late-collisional geodynamic settings as well as those generated at the late stages of evolution of hot rift structures).

Given the relatively low Y/Nb ratios (1.1–2.1), the studied rhyolites plot along, or below, the boundary between post-orogenic granites derived by partial melting of mafic lower continental crust or arc-type sources (A<sub>2</sub>-type) and granites related to sources analogous to those of the ocean island basalts, further modified by crystal fractionation (A<sub>1</sub>-type; Eby 1992; Fig. 7d). All these geochemical signatures correspond with other Permian acid igneous rocks generated in post-orogenic extensional tectonic environments from the southern Mongolia (e.g. Zhang et al. 2015, Blight et al. 2010a, b).

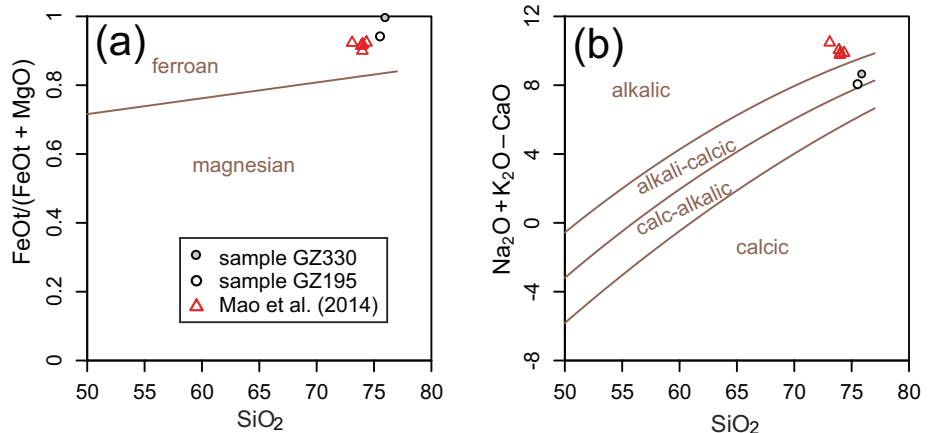


**Fig. 5** Whole-rock geochemical discrimination diagrams. **a** – FeO/(FeO + MgO) vs. SiO<sub>2</sub>. **b** –  $(Na_2O + K_2O - CaO)$  vs. SiO<sub>2</sub> (Frost et al. 2001).

**Tab. 3** Chemical composition of astrophyllite (wt. %), normalization scheme based on 26 O, 5 (OH + F)

	I	I	I	II	II
Nb <sub>2</sub> O <sub>5</sub>	6.44	5.32	4.76	2.51	4.09
SiO <sub>2</sub>	33.61	33.88	33.65	34.90	34.63
TiO <sub>2</sub>	5.10	4.74	4.90	8.22	7.24
ZrO <sub>2</sub>	3.45	4.90	5.00	2.55	2.07
Al <sub>2</sub> O <sub>3</sub>	1.35	1.24	1.10	0.97	1.17
V <sub>2</sub> O <sub>3</sub>	0.03	0.02	0.04	0.06	0.05
Cr <sub>2</sub> O <sub>3</sub>	0.01	0.01	0.01	0.00	0.00
MgO	0.02	0.00	0.01	0.01	0.01
CaO	0.24	0.24	0.45	0.69	0.36
MnO	1.66	1.50	1.46	1.46	1.63
FeO <sup>i</sup>	34.57	33.84	33.93	33.79	35.16
ZnO	0.36	0.28	0.34	0.32	0.41
Na <sub>2</sub> O	2.01	2.18	2.11	2.00	2.14
K <sub>2</sub> O	5.82	5.78	6.03	5.48	5.55
Rb <sub>2</sub> O	0.60	0.55	0.59	0.47	0.53
Cs <sub>2</sub> O	0.11	0.06	0.08	0.05	0.03
F	0.89	0.91	0.92	1.06	0.97
Cl	0.02	0.00	0.02	0.00	0.02
H <sub>2</sub> O	2.66	2.28	2.49	1.94	2.27
–O=F	0.38	0.38	0.39	0.45	0.41
Total	98.56	97.36	97.47	96.03	97.93
Nb	0.662	0.545	0.492	0.252	0.410
Si	7.640	7.668	7.704	7.745	7.693
Ti	0.872	0.807	0.845	1.372	1.210
Zr	0.383	0.541	0.558	0.276	0.224
Al	0.360	0.332	0.296	0.255	0.307
V	0.005	0.003	0.008	0.011	0.009
Cr	0.002	0.002	0.001	0.000	0.000
Mg	0.008	0.000	0.002	0.003	0.004
Ca	0.058	0.057	0.110	0.164	0.086
Mn	0.320	0.287	0.282	0.274	0.307
Fe	6.572	6.406	6.497	6.272	6.530
Zn	0.061	0.047	0.057	0.052	0.068
Na	0.885	0.958	0.936	0.859	0.921
K	1.687	1.670	1.762	1.550	1.573
Rb	0.087	0.080	0.087	0.067	0.075
Cs	0.011	0.006	0.008	0.005	0.003
Total	19.613	19.408	19.645	19.158	19.422
F	0.640	0.654	0.663	0.746	0.679
Cl	0.007	0.000	0.007	0.000	0.008
OH	4.028	3.438	3.796	2.865	3.359
O	26	26	26	26	26
Fe/(Fe+Mn)	0.954	0.957	0.958	0.958	0.955

#### 4.5. K–Ar dating

The studied sample (rhyolite GZ195) yielded an age of  $299.9 \pm 9.1$  Ma ( $1\sigma$ ), which falls close to the Carbonifer-

**Tab. 4** Analytical data for the K–Ar age determination

Analytical N <sup>o</sup>	Sample N <sup>o</sup>	K (wt. %)	<sup>40</sup> Ar <sub>rad</sub> (ccSTP/g)	<sup>40</sup> Ar <sub>rad</sub> (%)	K–Ar age (Ma)	error (Ma, $1\sigma$ )
8477	GZ195	3.555	$4.5086 \times 10^{-5}$	90.4	299.9	$\pm 9.1$

ous/Permian boundary (see Tab 4). Since this rhyolitic dyke does not exhibit any significant alteration, and forms a small intrusive body, the established K–Ar age should be considered the emplacement age.

## 5. Discussion and conclusions

The results of detailed study show that the rhyolite has an anomalous mineralogy with regard to the occurrence of Zr-rich alkali amphibole (riebeckite–arfvedsonite, possibly ferroleakeite) and astrophyllite. Astrophyllite has extremely high Fe<sup>i</sup>/(Fe<sup>i</sup> + Mn) ratio of 0.95–0.96 (Fig. 4), not yet reported in minerals of the astrophyllite group (cf. Piilonen et al. 2000, 2003).

The geological position and chemical composition of the studied rhyolite dyke (ferroan alkali-calcic metaluminous rhyolite) are consistent with post-collisional geodynamic settings described in literature (e.g. Sylvester 1989). Following the classification of A-type granites of Grebennikov (2014), and considering a scheme of the origin of A-type granitoids suggested by Frost and Frost (2011), the rhyolite studied shows features transitional between the A<sub>1</sub>-type and A<sub>2</sub>-type granites. The relatively low Y/Nb ratios of 1.1 and 2.1, and high Cr contents (up to 90 ppm) indicate that the rock may represent a differentiate of a mantle-derived, alkali basalt magma (e.g. Eby 1992; Frost and Frost 2011). As shown by Eby (1992), crustal contamination of A<sub>1</sub> group granitic magmas may increase Y/Nb ratio so that it plots in the A<sub>2</sub> field.

The negative Ti, Ba, Sr, P and Eu anomalies in the multielement plot (Fig. 6a) can be interpreted as a result of fractionation of feldspars, apatite and Ti-rich minerals. The lanthanide tetrad effect is usually reported from highly evolved granites (Bau 1996) and indicates a fluid/melt interaction within this system (Irber 1999). According to Yang et al. (2014), formation of hydrothermal and metamict zircons can be responsible for the origin of the M-type tetrad effect. Fluid interaction in the late- or post-magmatic phase is also supported by secondary enrichment of the alkali amphibole with Zr. Increased oxygen fugacity during the terminal phases of hydrothermal process is indicated by crystallization of hematite in miarolitic cavities, whereas the rock itself contains accessory ilmenite.

The conventional K–Ar geochronology of the sample studied yielded  $299.9 \pm 9.1$  Ma, indicating latest Carboniferous or Early Permian igneous activity. A recently studied Early Permian peralkaline rhyolite from southern Altai exhibits similar petrology, chemical composition and tectonic setting, and a very

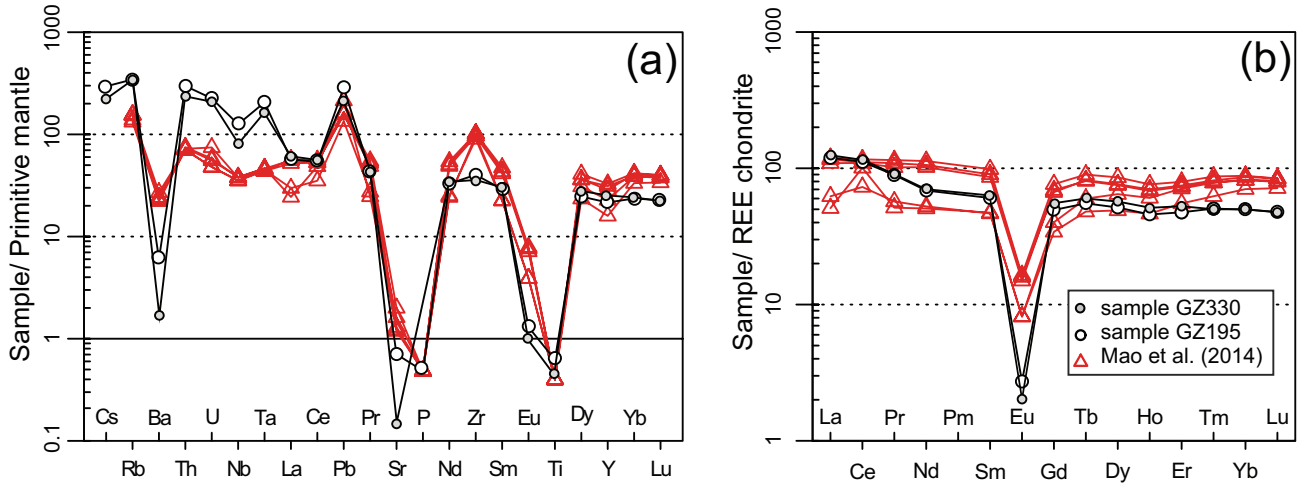


**Fig. 6** Multi-element diagrams. **a** – Primitive mantle normalized pattern. **b** – Chondrite-normalized REE pattern. Normalizing values are taken from McDonough and Sun (1995) and Boynton (1984), respectively.

similar age ( $286.5 \pm 2.1$  and  $286.7 \pm 2.1$  Ma – Mao et al. 2014).

The presence of  $A_1$ -type volcanism gives evidence of early Permian extension in the western Mongolian Altai, which can be related to initial rifting (see. e.g. Eby 1992; Bonin 2007).

sample preparation for K–Ar geochronology. The authors are also grateful to reviewers Paula Pilonen and Elena Sokolova and to chief editor Vojtěch Janoušek for suggested improvements and to Jaroslav Hak for the correction of the language.

**Acknowledgments.** This study was supported by the Czech Development Agency project “Geological mapping 1 : 50 000 and assessment of economic potential of selected region in Western Mongolia” CzDA-RO-MN-2013-1-32220. The authors are grateful to Pavel Čáp, Tomáš Vorel, Igor Soejono, Kryštof Verner, Bayart Nadmid and Soyol-Erdene Ulziisuren for invaluable field assistance, to Stanislav Vrána for microscopic studies of rocks and to Vladislav Rapprich for his assistance in

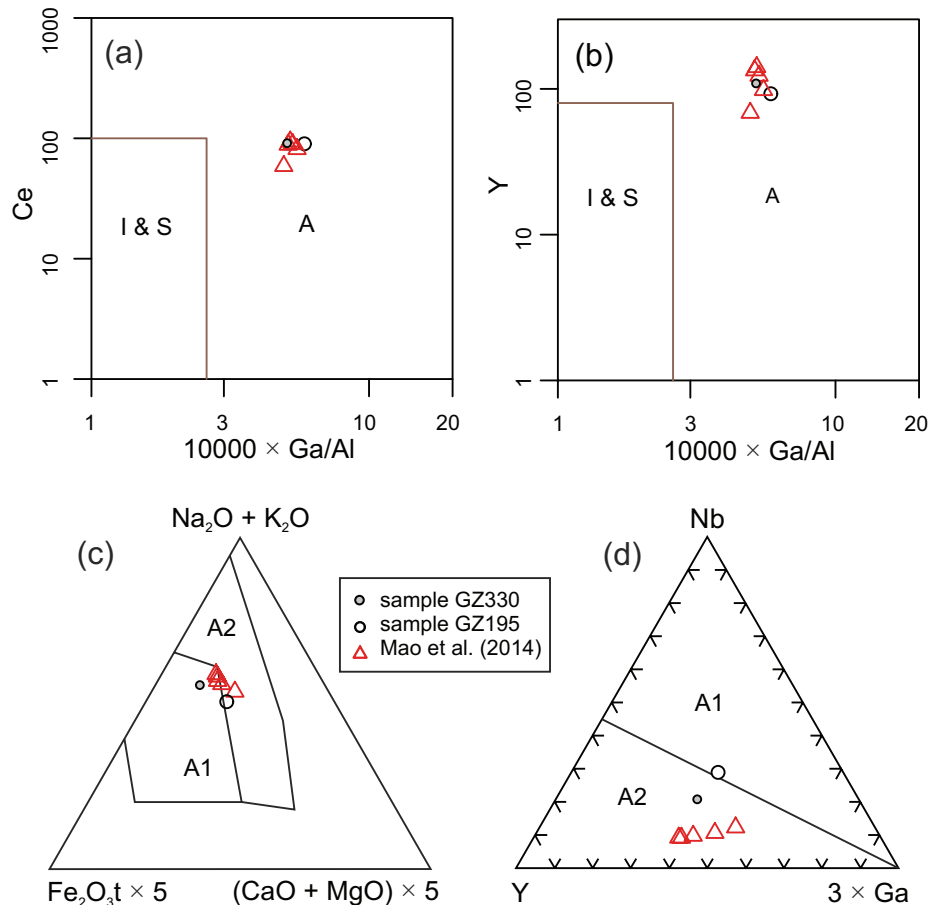


**Fig. 7** Whole-rock geochemical discrimination diagrams. **a** and **b** vs.  $10000 \times \text{Ga}/\text{Al}$  after Whalen et al. (1987), showing the fields of I-, S-, and A-type granites. **c** – Ternary plot  $\text{Fe}_2\text{O}_3 \times 5 - (\text{Na}_2\text{O} + \text{K}_2\text{O}) - (\text{CaO} + \text{MgO}) \times 5$  for classification of A-type (ferroan) granites, (after Grebennikov 2014). **d** – Ternary plot  $\text{Y} - \text{Nb} - 3 \times \text{Ga}$  for classification of A-type granites (Eby 1992).

## References

- BAATARHUYAG A, GANSUKH L (1999) Geological map 1:200 000, L-46-IX, L-46-II-G. Unpublished Manuscript, Geofond, Ulaanbaatar
- BADARCH G, CUNNINGHAM CW, WINDLEY BF (2002) A new terrane subdivision for Mongolia: implications for the Phanerozoic crustal growth of Central Asia. *J Asian Earth Sci* 21: 87–110
- BALOGH K (1985) K/Ar dating of Neogene volcanic activity in Hungary: experimental technique, experiences and methods of chronologic studies. *ATOMKI Rep. D/1*: 277–288
- BAU M (1996) Controls on the fractionation of isoivalent trace elements in magmatic and aqueous systems: evidence from Y/Ho, Zr/Hf, and lanthanide tetrad effect. *Contrib Mineral Petrol* 123: 323–333
- BLIGHT JHS, CROWLEY QG, PETTERSON MG, CUNNINGHAM D (2010a) Granites of the southern Mongolia Carboniferous arc: new geochronological and geochemical constraints. *Lithos* 116: 35–52
- BLIGHT JHS, PETTERSON MG, CROWLEY QG, CUNNINGHAM D (2010b) The Oyut Ulaan volcanic group: stratigraphy, magmatic evolution and timing of Carboniferous arc development in SE Mongolia. *J Geol Soc, London* 167: 491–509
- BONIN B (2007) A-type granites and related rocks: evolution of a concept, problems and prospects. *Lithos* 97: 1–29
- BONIN B (2008) Death of super-continent and birth of oceans heralded by discrete A-type granite igneous events: the case of the Variscan–Alpine Europe. *J Geosci* 53: 237–252
- BOYNTON WV (1984) Cosmochemistry of the rare earth elements: meteorite studies. In: HENDERSON P (ed) *Rare Earth Element Geochemistry*. Elsevier, Amsterdam, pp 63–114
- BURIÁNEK D, HANŽL P, BUDIL P, GERDES A (2012) Evolution of the early Permian volcanic–plutonic complex in the western part of the Permian Gobi-Altay rift (Khar Argalant Mts., SW Mongolia). *J Geosci* 57: 105–126
- BUSLOV MM, SAFONOVA IY, WATANABE T, OBUT OT, FUJIWARA Y, IWATA K, SEMAKOV NN, SUGAI Y, SMIRNOVA LV, KAZANSKY AY (2001) Evolution of the Paleo-Asian Ocean (Altai-Sayan Region, Central Asia) and collision of possible Gondwana-derived terranes with the southern marginal part of the Siberian Continent. *Geosci J* 5: 203
- CHEN B, ARAKAWA Y (2005) Elemental and Nd–Sr isotopic geochemistry of granitoids from the West Junggar foldbelt (NW China), with implications for Phanerozoic continental growth. *Geochim Cosmochim Acta* 69: 1307–1320
- CHEN B, JAHN BM (2004) Genesis of post-collisional granitoids and basement nature of the Junggar Terrane, NW China: Nd–Sr isotopic and trace element evidence. *J Asian Earth Sci* 23: 691–703
- COX AV, DALRYMPLE GB (1967) Statistical analysis of geomagnetic reversal data and the precision of potassium–argon dating. *J Geophys Res* 72: 2603–2614
- EBY GN (1992) Chemical subdivision of the A-type granitoids: petrogenetic and tectonic implications. *Geology* 20: 641–644
- FROST CD, FROST BR (2011) On ferroan (A-type) granitoids: their compositional variability and modes of origin. *J Petrol* 52: 39–53
- FROST BR, BARNES CG, COLLINS WJ, ARCULUS RJ, ELLIS DJ, FROST CD (2001) A geochemical classification for granitic rocks. *J Petrol* 42: 2033–2048
- GREBENNIKOV AV (2014) A-type granites and related rocks: petrogenesis and classification. *Russ Geol Geophys* 55: 1354–1356
- IRBER W (1999) The lanthanide tetrad effect and its correlation with K/Rb, Eu/Eu\*, Sr/Eu, Y/Ho, and Zr/Hf of evolving peraluminous granite suites. *Geochim Cosmochim Acta* 63: 489–508
- JAHN BM (2004) The Central Asian Orogenic Belt and growth of the continental crust in the Phanerozoic. In: MALPAS J, FLETCHER CJN, ALI JR, AITCHISON JC (eds) *Aspects of the Tectonic Evolution of China*. Geological Society of London Special Papers 226: 73–100
- JAHN BM, WU FY, CHEN B (2000) Granitoids of the Central Asian Orogenic Belt and continental growth in the Phanerozoic. *Trans Roy Soc Edinb, Earth Sci* 91: 181–193
- JANOŮŠEK V, FARROW CM, ERBAN V (2006) Interpretation of whole-rock geochemical data in igneous geochemistry: introducing Geochemical Data Toolkit (GCDkit). *J Petrol* 47: 1255–1259
- JIANG YD, SUN M, ZHAO GC, YUAN C, XIAO W, XIA XP, LONG XP, WU FY (2010) The ~390 Ma high-T metamorphic event in the Chinese Altai: a consequence of ridge-subduction? *Amer J Sci* 310: 1421–1452
- JIANG YD, SUN M, KRÖNER A, TUMURKHUU D, LONG XP, ZHAO GC, YUAN C, XIAO WJ (2012) The high-grade Tsel Terrane in SW Mongolia: an Early Paleozoic arc system or a Precambrian sliver? *Lithos* 142–143: 95–115
- KAPUSTIN YL (1972) Zircophyllite – the zirconium analogue of astrophyllite. *Zap Vses Mineral Obschch* 101: 459–463 (in Russian)
- KOVALENKO VI, YARMOLYUK VV, KOVACH VP, KOTOV AB, KOZAKOV IK, SALNIKOVA EB (1996) Sources of Phanerozoic granitoids in Central Asia: Sm–Nd isotope data. *Geochem Int* 34: 628–640
- KRÖNER A, LEHMANN J, SCHULMANN K, DEMOUX A, LEXA O, TOMURKHUU D, ŠTÍPSKÁ P, LIU D, WINGATE MTD (2010) Lithostratigraphic and geochronological constraints on the evolution of the Central Asian Orogenic Belt in SW Mongolia: Early Paleozoic rifting followed by Late Paleozoic accretion. *Amer J Sci* 310: 523–574
- LITVINOVSKY BA, JAHN BM, ZANVILEVICH AN, SAUNDERS A, POULAIN S, KUZMIN DV, REICHOW MK, TITOV AV (2002)

- Petrogenesis of syenite-granite suites from the Bryansky Complex (Transbaikalia, Russia): implications for the origin of A-type granitoid magmas. *Chem Geol* 189: 105–133
- LIU W, LIU XJ, LIU LJ (2013) Underplating generated A- and I-type granitoids of the East Junggar from the lower and the upper oceanic crust with mixing of mafic magma: insights from integrated zircon U–Pb ages, petrography, geochemistry and Nd–Sr–Hf isotopes. *Lithos* 179: 293–319
- LONG X, YUAN C, SUN M, XIAO W, ZHAO G, WANG Y, CAI K, XIA X, XIE L (2009) Detrital zircon ages and Hf isotopes of the early Paleozoic flysch sequence in the Chinese Altai, NW China: new constrains on depositional age, provenance and tectonic evolution. *Tectonophysics* 480: 213–231
- MAO QG, XIAO WJ, FANG TH, WINDLEY BF, SUN M, AO SJ, ZHANG JE, HUANG XK (2014) Geochronology, geochemistry and petrogenesis of Early Permian alkaline magmatism in the Eastern Tianshan: implications for tectonics of the Southern Altaids. *Lithos* 190–191: 37–51
- MERLET C (1994) An accurate computer correction program for quantitative electron probe microanalysis. *Microchim Acta* 114/115: 363–376
- MCDONOUGH WF, SUN SS (1995) The composition of the Earth. *Chem Geol* 120: 223–253
- PIILONEN PC, LALONDE AE, McDONALD AM, GAULT RA (2000) Niobokupletskite, a new astrophyllite-group mineral from Mont Saint-Hilaire, Quebec, Canada: description and crystal structure. *Canad Mineral* 38: 627–639
- PIILONEN PC, LALONDE AE, McDONALD AM, GAULT RA, LARSEN AO (2003) Insights into the astrophyllite group I. Nomenclature, composition and development of a standardized general formula. *Canad Mineral* 41: 1–26
- SOKOLOVA E (2012) Further developments in the structure topology of the astrophyllite-group minerals. *Mineral Mag* 76: 863–882
- SOEJONO I, BURIÁNEK D, SVOJTKA M, ŽÁČEK V, ČÁP P, JANOUŠEK V (2016) Mid-Ordovician and Late Devonian magmatism in the Togtokhinshil Complex: new insight into the formation and accretional evolution of the Lake Zone (Western Mongolia). *J Geosci* 61: 5–23
- STEIGER RH, JÄGER E (1977) Subcommittee on Geochronology: convention on the use of decay constants in geo- and cosmochronology. *Earth Planet Sci Lett* 36: 359–362
- SUN M, YUAN C, XIAO W, LONG XIA X, ZHAO G, LIN S, WU F, KRÖNER A (2008) Zircon U–Pb and Hf isotopic study of gneissic rocks from the Chinese Altai: progressive accretionary history in the early to middle Palaeozoic. *Chem Geol* 247: 352–383
- SYLVESTER PJ (1989) Post-collisional alkaline granites. *J Geol* 97: 261–280
- ŞENGÖR A, NATAL'IN B, BURTMAN V (1993) Evolution of the Altaid tectonic collage and Paleozoic crustal growth in Eurasia. *Nature* 364: 299–307
- TOMURTOGОО O (1997) A new tectonic scheme of the Paleozooids in Mongolia. *Mongolian Geoscientist* 3: 12–17
- WANG Q, WYMAN DA, ZHAO ZH, XU JF, ZHENG HB, XIONG XL, DAI DX, LI HC, CHU ZY (2007) Petrogenesis of Carboniferous adakites and Nb-enriched arc basalts in the Alataw area, northern Tianshan range (western China): implications for Phanerozoic crustal growth in the Central Asia Orogenic Belt. *Chem Geol* 236: 42–64
- WANG ZG, CHEN YL, DONG ZS, WU MQ, ZHANG J (1993) The high-alkaline intrusive rock belts in northern Xinjiang: their geology, geochemistry and genesis. In: TU GZ (ed) *Progress of Solid-Earth Sciences in Northern Xinjiang, China*. Science Publishing House, Beijing, 163–172 (in Chinese)
- WHALEN JB, CURRIE KL, CHAPPELL BW (1987) A-type granites: geochemical characteristics, discrimination and petrogenesis. *Contrib Mineral Petrol* 95: 407–419
- WU FY, SUN DY, LI HM, JAHN BM, WILDE SA (2002) A-type granites in northeastern China: age and geochemical constraints on their petrogenesis. *Chem Geol* 187: 143–173
- XIAO WJ, WINDLEY BF, BADARCH G, SUN S, LI J, QIN K, WANG Z (2004) Palaeozoic accretionary and convergent tectonics of the southern Altaids: implications for the growth of central Asia. *J Geol Soc, London* 161: 1–4
- YANG W-B, NIU HC, SHAN Q, SUN WD, ZHANG H, LI NB, JIANG YH, YU XY (2014) Geochemistry of magmatic and hydrothermal zircon from the highly evolved Baerzhe alkaline granite: implications for Zr–REE–Nb mineralization. *Miner Depos* 49: 451–470
- ZHANG X, YUAN L, XUE F, YAN X, MAO Q (2015) Early Permian A-type granites from central Inner Mongolia, north China: magmatic tracer of post-collisional tectonics and oceanic crustal recycling. *Gondwana Res* 28: 311–327
- ZONENSHAIN LP, KUZMIN MI, NATAPOV LM (1990) *Geology of the USSR: A Plate-Tectonic Synthesis*. American Geophysical Union, Geodynamics Series V 21, Washington, DC, pp 1–242

